Conformational Change of the Hairpin-like-structured Robo2 Ectodomain Allows NELL1/2 Binding

Masaki Miyaguchi[1], Yoichi Nakanishi[1], Andrés D. Maturana[1], Kimihiko Mizutani[2], and Tomoaki Niimi[1]*

[1]Graduate School of Bioagricultural Sciences, Nagoya University, Nagoya, Japan

[2]Graduate School of Agriculture, Kyoto University, Kyoto, Japan

*Correspondence to be addressed to : Tomoaki Niimi, Graduate School of Bioagricultural Sciences, Nagoya University, Furo-cho, Chikusa-ku, Nagoya 464-8601, Japan; tniimi@agr.nagoya-u.ac.jp; Tel. 81-52-789-5015

Abbreviations: ECD, ectodomain; EGFL, epidermal growth factor-like; FNIII, fibronectin type III; FRET, Förster resonance energy transfer; Ig, immunoglobulin-like; LG, laminin G; NELL, neural epidermal growth factor-like (NEL)-like; Robo, Roundabout; SEC, size exclusion chromatography; VWC, von Willebrand factor type C

Abstract

Since neural epidermal growth factor-like-like (NELL) 2 was identified as a novel ligand for the roundabout (Robo) 3 receptor, research on NELL–Robo signaling has become increasingly important. We have previously reported that Robo2 can bind to NELL1/2 in acidic conditions but not at neutral pH. The NELL1/2-binding site that is occluded in neutral conditions is thought to be exposed by a conformational change of the Robo2 ectodomain upon exposure to acidic pH; however, the underlying structural mechanisms are not well understood. Here, we investigated the interaction between the immunoglobulin-like domains and fibronectin type III domains that form hairpin-like structure of the Robo2 ectodomain, and demonstrated that acidic pH attenuates the interaction between them. Alternative splicing isoforms of Robo2, which affect the conformation of the hairpin-like structure, were found to have distinct NELL1/2-binding affinities. We developed Förster resonance energy transfer-based indicators for monitoring conformational change of the Robo2 ectodomain by individually inserting donor and acceptor fluorescent proteins at its ends. These experiments revealed that the ends of the Robo2 ectodomain are close to each other in acidic conditions. By combining these findings with the results of size exclusion chromatography analysis, we suggest that, in acidic conditions, the Robo2 ectodomain has a compact conformation with a loose hairpin-like structure. These results may help elucidate the signaling mechanisms resulting from the interaction between Robo2 and NELL1/2 in acidic conditions.

Keywords: cell surface receptor, protein conformation, protein domain, protein-protein interaction, structural model

Introduction

Roundabout (Robo) receptors and their Slit ligands are well known axon guidance molecules that were originally identified in *Drosophila* mutants with commissural axon pathfinding defects.[1,2] Slit–Robo signaling was first established in the development of the nervous system, but has also been shown to function in a number of developmental events outside the nervous system.[3,4] In mammals, there are four Robo receptors (Robo1–4) and three Slit ligands (Slit1–3).[5-7] Robo1–3 share five immunoglobulin-like (Ig) and three fibronectin type III (FNIII) domains in their ectodomain, whereas Robo4, an endothelial-specific member of the Robo family, contains only two Ig and two FNIII domains in its ectodomain. Robo1 and Robo2 have the binding site for Slit proteins in their first Ig (Ig1) domain,[8,9] but Robo3 has lost the ability to bind Slit proteins because of a few amino acid changes in its Ig1 domain.[10] Instead, neural epidermal growth factor-like (NEL)-like (NELL) 2 was identified as a ligand for Robo3, thereby functioning as a negative regulator of Robo1/2-mediated repulsion from the midline in pre-crossing axons.[11] Although the divergent family member NELL1 also binds to Robo3, NELL1 has little if any effect on commissural axon repulsion.[11,12]

The *Nel* gene was first isolated from an embryonic chicken cDNA library, and was named because it contains six epidermal growth factor-like (EGFL) repeats and it is expressed in neural tissues.[13] Two novel genes homologous to the chicken *Nel* gene were later isolated from a human brain cDNA library, and were designated *Nel-like 1* and *Nel-like 2* (*NELL1/2*).[14] NELL1 and NELL2 constitute a NELL family of secretory glycoproteins that contain a laminin G (LG) domain, four von Willebrand factor type C domains, and six EGFL repeats.[15,16] Both NELL1 and NELL2 are expressed primarily in the brain, and have high similarity in their amino acid sequences and domain structures.[17,18] Nevertheless, the biological functions of these proteins are quite different: NELL1 functions as a regulator of craniofacial skeletal morphogenesis,[19,20] and NELL2 plays multiple roles such as in neuronal development,[21-23] sperm maturation,[24] and cancer progression.[25] The difference in these functions may be due to the difference in the binding properties of NELL1 and NELL2 to their receptors. NELL1 targets β1 integrin and contactin-

associated protein-like 4 (Cntnap4) as cell surface receptors,[26,27] whereas the known receptors for NELL2 include Robo3 and an orphan receptor tyrosine kinase, c-ros oncogene 1 (ROS1).[11,24]

We have previously shown that NELL1/2 bind to the first FNIII (FNIII1) domain of Robo2 in acidic conditions.[28] The idea that the NELL1/2-binding site of Robo2 is occluded in neutral conditions is consistent with the report of Barak *et al.* on the crystal structure of the Robo2 ectodomain that has a hairpin-like architecture in which the Ig4 and Ig5 domains mask the FNIII1 domain.[29] However, it is not clear how the NELL1/2-binding site is exposed in acidic conditions. Local extracellular acidification has been observed in pathological conditions, such as ischemia and inflammation during bone fractures.[30] It is generally known that metabolic acidosis causes a decrease in the bone mineral density by inducing cell death of osteoblasts and activation of osteoclasts to resorb bone. [31,32] However, recent study indicated that short-term acidic stimulation enhances the stem cell phenotype of mesenchymal stem cells, which facilitates differentiation to osteoblasts.[33] From these findings, we hypothesized that the temporal interaction between NELL1 and Robo2 in osteoblast precursors in acidic conditions may contribute to enhance bone formation during bone tissue healing.

To gain more detailed understanding of NELL1/2-Robo2 interactions, we carried out solid-phase binding assays to investigate the interaction between the Ig domains and FNIII domains of Robo2, and demonstrated that it was attenuated following the shift from neutral to acidic pH, indicating that the NELL1/2-binding site is exposed in acidic conditions. Analysis of the microexon 6b− (e6b−) isoform of Robo2, an alternative splicing isoform lacking four amino acids in the linker region between the Ig3 and Ig4 domains, revealed that its NELL1/2-binding affinity is higher than that of the microexon 6b+ (e6b+) isoform. To monitor conformational change of the Robo2 ectodomain, we developed Förster (or fluorescence) resonance energy transfer (FRET)-based indicators by inserting FRET donor and acceptor proteins at the respective ends of the Robo2 ectodomain. Acid treatment increased FRET ratios, indicating that the ends of the Robo2 ectodomain come close to each other in acidic conditions while the protein maintained the hairpin-like structure. In contrast, the FRET construct of the e6b− isoform showed decreased FRET ratios in both neutral and acidic conditions, suggesting that the distance between the ends of the

Robo2 ectodomain was increased compared with the e6b+ isoform. Size exclusion chromatography (SEC) analysis showed that the Robo2 ectodomain may have a more compact conformation in acidic conditions than in neutral conditions, while the Robo2 ectodomain of the e6b− isoform may have a bulkier conformation than that of the e6b+ isoform in neutral conditions. These results reveal the biochemical and structural mechanisms by which conformational change in the Robo2 ectodomain allows NELL1/2 binding.

Results

Acidic pH exposes the NELL1/2-binding site of the Robo2 ectodomain, which allows binding to NELL1

To investigate how the interaction between NELL1 and the Robo2 ectodomain, and how the interaction between the Ig and the FNIII domains of Robo2, change in response to acidic pH, we carried out solid-phase binding assays using buffers in the neutral to acidic pH range (Figures 1 and S1). The NELL1-binding affinity of the Robo2 ectodomain gradually increased as the pH was decreased from 7.4 to 5.5. The binding between the Ig and the FNIII domains of Robo2 gradually decreased in this pH range. Previous studies have shown that the acidic pH range examined does not affect the binding affinity between NELL1 and the FNIII domains of Robo2.[28] Therefore, it is considered that acidic pH has an influence on the conformation of the whole Robo2 ectodomain containing the Ig domains. Collectively, these results suggest that acidic pH alters the charge of amino acids in the binding interface between the Ig and the FNIII domains of Robo2, causing conformational change that exposes the NELL1/2-binding site on the FNIII1 domain.

The Robo2 e6b− splicing isoform shows higher affinity for NELL1/2 than the e6b+ isoform in acidic conditions

Recently, it was shown that the mammalian *Robo2* gene undergoes alternative splicing to produce several isoforms with complex expression patterns and axon guidance activities.[34] Among them, alternative splicing isoforms of microexon 6b, which is 12-bp long, in the *Robo2* gene result in a four amino acids

insertion/deletion between the Ig3 and Ig4 domains and are therefore referred as the e6b+ and e6b− isoforms, respectively (Figure 2(A) and (B)).[34] Semi-quantitative RT-PCR analysis using cDNAs prepared from various human and mouse tissues and primers designed to sandwich microexon 6b indicated that the expression level of the e6b− isoform was much lower than that of the e6b+ isoform in most tissues (Figure 2(C) and (D)).

Because the domain composition of the Ig domains has a great influence on their binding to the FNIII domains (Figure S2), we investigated whether the two splicing isoforms, e6b+ and e6b−, have different binding properties (Figure 3). Because the Robo2 isoform we originally investigated was e6b+, we prepared a set of expression vectors for the e6b− isoform by inverse PCR. Although there was not much difference in NELL1-binding affinity between the two isoforms around neutral pH, a significant difference was observed in acidic conditions (Figure 3(A)). The calculated apparent K_D values of the e6b+ and e6b− isoforms for binding to NELL1 at pH 5.5 were 205 nM and 53.4 nM, respectively (Figure 3(B)). The higher affinity of the e6b− isoform for NELL1 can be explained by the weak binding affinity of the Ig domains to the FNIII domains (Figure 3(C)). A single amino acid substitution mutant of the e6b+ isoform, L398R, in which a leucine residue at the interface between the Ig4 and the FNIII1 domains was substituted with arginine,[29] showed a similar result to that for the e6b− isoform, i.e., weak binding affinity of the Ig domains to the FNIII domains (Figure 3(C)). When combined with previous data showing that NELL1 can bind to the L398R mutant of Robo2 even in neutral conditions,[28] these results further support the idea that conformational change in the hairpin-like structure formed by the Ig and FNIII domains of Robo2 allows NELL1/2 binding. The NELL1-binding affinity for membrane-bound Robo2 also seems to be slightly higher for the e6b− isoform than for the e6b+ isoform (Figure 3(D)). There was no difference in the transport of the isoforms to the cell surface (Figure S1(F)). Note that the e6b− isoform had higher binding affinity than e6b+ isoform for NELL2 as well as for NELL1 (Figure S3).

FRET-based indicators to assess the topological conformation of the Robo2 ectodomain

To investigate the conformational change of the Robo2 ectodomain in acidic conditions, we developed an intramolecular FRET sensor for the Robo2 ectodomain. The cyan fluorescent protein (CFP)−yellow fluorescent protein (YFP) pair is commonly used for FRET analysis,[35] but, as far as we know, no acid-tolerant YFP has been found,[36] so the CFP−green fluorescent protein (GFP) pair was selected. Acid-tolerant fluorescent proteins mTurquoise2/CFP and Gamillus/GFP[37,38] were used as the donor and acceptor, and were fused to the *C*- and *N*-termini of the Robo2 ectodomain (ECD), respectively (Figure 4(A) and (B)). The chimeric proteins (Gam:Robo2-ECD:mTq2) were excited at 430 nm (λ_{max} for mTurquoise2), and the emission spectrum was measured at 460−560 nm. When the chimeric proteins encompassing the entire Robo2 ectodomain were assayed, the emission spectrum was not much different from that of control protein consisting only of the CFP derivative Cerulean, and there was little increase in the emission peak of the acceptor at 515 nm (λ_{max} for Gamillus) (Figure S4). So, given that the distance between the two fluorophores was not short enough to cause FRET, we created deletion constructs of the Ig1 domain and/or the FNIII3 domain of Robo2 to decrease the distance between the fluorophores. These domains are not directly involved in the formation of the hairpin-like structure,[29] and the binding affinity between the Ig2−5 domains and the FNIII1−2 domains was sufficiently maintained after the deletion of the Ig1 and FNIII3 domains (Figure S2). The Ig1 domain deletion construct gave a similar result to that for the entire Robo2 ectodomain (Figure S4). However, the construct in which both the Ig1 and the FNIII3 domains were deleted (Gam:Robo2-ECD/ΔIg1&FNIII3:mTq2) clearly showed an increase in the emission peak from the acceptor and a quenching of donor emission (Figure 4(C)). The calculated FRET ratio (the emission intensity of Gamillus/GFP divided by the emission intensity of mTurquoise2/CFP) significantly increased (Figure 4(D)), indicating that the two fluorophores were close enough to be able to assess the conformation of the Robo2 ectodomain. Therefore, this FRET construct was used for subsequent experiments.

Acidic pH induces conformational change of the Robo2 ectodomain to form compact structures

To analyze the conformational change of the Robo2 ectodomain in acidic conditions, the Gam:Robo2-ECD/ΔIg1&FNIII3:mTq2 protein was treated with buffers at acidic pH and its emission

spectra were measured (Figure 5). The emission peak gradually increased as the pH was decreased from 7.4 to 5.5, suggesting that the distance between the two fluorophores decreased. We next prepared a Gam:Robo2-ECD/ΔIg1&FNIII3:mTq2 construct for the e6b− isoform by inverse PCR and measured its emission spectrum in neutral conditions (Figure 6). The emission peak of the e6b− isoform was less intense than that of the e6b+ isoform at neutral pH. The L398R mutant of the e6b+ isoform showed a similar result to that for the e6b− isoform, suggesting that the distance between the two fluorophores was greater in these FRET constructs than in the wild-type e6b+ isoform; the FRET ratio did not increase even when these FRET constructs were measured in acidic conditions (Figure S5).

The purified Robo2 ectodomains without fluorescent protein tags were also analyzed by SEC to assess their conformations (Figure 7). The SEC profiles revealed that almost all of the Robo2 ectodomains exist as dimers. The e6b+ isoform eluted a little earlier at pH 7.4 than at pH 5.5. The difference in elution peak volume was quite small, but the reproducibility of the elution pattern was observed (Figure S6). It should be noted that this result may represent a change in the ratio of monomer-dimer equilibrium, but it may also suggest a more compact conformation was formed at pH 5.5. The SEC profiles of the e6b− isoform and the L398R (e6b+) mutant at neutral pH revealed that these proteins eluted a little earlier than the wild-type e6b+ isoform. These results may suggest that they had a bulkier conformation than the latter (Figures 7 and S6).

Discussion

Here, we first investigated the interaction between NELL1 and the Robo2 ectodomain, and the intramolecular interaction between the Ig domains and the FNIII domains of Robo2, using cell-free binding assays—these interactions were found to show opposite responses in the neutral to acidic pH range (Figure 1). We have previously shown that the Ig domains of Robo2 bind to the FNIII domains in neutral conditions, but did not clearly show whether the binding between the Ig domains and the FNIII domains dissociates in acidic conditions.[28] Consequently, the relationship between the NELL1-binding affinity and the conformational change of the Robo2 ectodomain in acidic conditions could not be well explained. In the

present study, we succeeded in evaluating the protein interactions in response to pH changes by improving the assay conditions from the previous study. That is, the neutral buffer in the binding assay was changed from HBAH [containing bovine serum albumin (BSA)] to HEPES (not containing BSA) to facilitate comparison with the effect in the acidic MES buffer (not containing BSA). As a result, we suggest that acidic pH attenuates the intramolecular interaction between the Ig domains and the FNIII domains of Robo2, which changes the conformation of the Robo2 ectodomain and enables access to NELL1. Comparing the three-dimensional structure around the FNIII1 domain within the hairpin-like-structured ROBO2 ectodomain and the NELL1-binding sites of the human ROBO3-FNIII1 domain,[12,29] it is presumed that part of the NELL1-binding site of ROBO2 is masked in neutral conditions (Figure S7). Further structural studies are required to elucidate a three-dimensional structure of the Robo2 ectodomain that allows access to NELL1 in acidic pH conditions.

An intramolecular FRET biosensor can serve as a tool to monitor conformational change of a sensor domain.[39,40] Because the energy transfer depends on the orientation and distance between the two fluorophores, extensive trial-and-error is required to find a suitable spatial arrangement for FRET to occur in an intramolecular FRET sensor. We were able to observe FRET signals in the Robo2 ectodomain construct in neutral conditions after deleting the Ig1 and the FNIII3 domains, and the signal further increased in acidic conditions (Figures 4 and 5). However, the FRET analysis alone cannot distinguish which of the distance and the orientation had the greater effect. Therefore, we also performed SEC analysis and found that the Robo2 ectodomain eluted a little earlier at neutral pH than at acidic pH. In our SEC analysis, the Robo2 ectodomain proteins are always eluted with a size consistent with them being dimers,[28] then this peak shift may represent a change in the ratio of monomer-dimer equilibrium. Although further analysis is needed to eliminate the effects of dimerization, it may suggest that a more compact conformation was formed in acidic conditions (Figure 7). Taken together, these results indicate that the distance between the two fluorophores became shorter and the hairpin-like structure was loosened in acidic conditions (Figure 8). The decreased FRET ratio and the SEC profile for both the e6b− isoform and the L398R mutant of the e6b+ isoform suggest that, in these two cases: 1) The hairpin-like structure is more twisted while the

NELL1/2-binding site is exposed, resulting in an increase in the distance between the two fluorophores; or 2) the hairpin-like structure is completely unwound to form an extended conformation, resulting in an increase in the distance between the fluorophores. The former is more likely, because the crystal structure of the Robo2 ectodomain revealed by Barak *et al*. was of the e6b− isoform.[29] The finding that our FRET construct of the e6b− isoform did not show an increase in the FRET ratio in acidic conditions was probably because of a poor orientation of two fluorophores rather than the distance between them (Figure S5). This may indicate that in the FRET construct of the e6b+ isoform, the insertion of four amino acids between the Ig3 and Ig4 domains serves as a flexible linker that allows the N-terminus to move closer to the C-terminus. Improvement of the FRET construct, such as by insertion of appropriate spacer sequences between the ends of the Robo2 ectodomain and the fluorophores, may decrease the effect of orientation.

Several studies have reported a relationship between the oligomerization state of Robo receptors and the ligand-induced activation mechanism.[29,41-43] Barak *et al.* suggested that Slit-binding induces a change in the oligomerization state of Robo2 from a *trans*-homodimer where the Ig1 domain of one molecule binds to the Ig5 domain of a reciprocal one, which is an inactive form, to an Ig4-mediated *cis*-homodimer with an open conformation, which is an active form.[29] Recently, Pak *et al.* revealed that the Robo3 ectodomain mostly exists as a monomer and has an open conformation,[12] which is consistent with the result that NELL1/2 interacts with Robo3 in neutral conditions.[28] They also speculated that NELL1/2 may regulate the conformational change of Robo1/2.[12] Because our successful FRET construct lacks the Ig1 domain, which is the binding site for Slit ligands, conformational change of the Robo2 ectodomain following Slit-binding cannot be examined. Although it is a preliminary experiment, when NELL1 protein was mixed with the FRET construct in acidic conditions, the FRET ratio did not change (Figure S8), suggesting that NELL1 does not cause the Robo2 ectodomain to form an open conformation. Further analysis is needed to confirm this result, but it may suggest a difference in the activation mechanism between the Slit–Robo and the NELL–Robo signaling.

Mammalian *Robo1* and *Robo2* genes share an alternative microexon 6b, which is 9 bp and 12 bp long, respectively.[34] Johnson *et al.* demonstrated that the splicing isoforms of microexon 6b in both *Robo1/2*

genes display distinct axon guidance activities and Slit signaling properties. However, the underlying causes of these differences remain elusive because of similar binding affinities to Slit proteins of these splicing isoforms.[34] We have identified that the Robo2 e6b− isoform has higher binding affinity for NELL1/2 than the e6b+ isoform because of the lower binding affinity of the Ig domains to the FNIII domains in the former (Figure 2). According to the crystal structure of the Robo2 ectodomain, the four amino acids encoded by microexon 6b do not appear to directly interact with the FNIII domains. Binding assays using various fragments of the Ig domains and the FNIII domains showed that domains Ig1−3 are important for the interaction with the FNIII domains (Figure S2). Taken together, these results suggest that the overall conformation of the Ig1−5 domains contributes to the conformation of the hairpin-like structure of the Robo2 ectodomain. Furthermore, the conformation of the hairpin-like structure may contribute to the formation of *cis*- and *trans*-homodimers of Robo1/2, thereby affecting the activation of receptors and downstream signaling. Although this is only speculation at this point, the difference in the axon guidance activities and signaling properties of the splicing isoforms may be partly due to conformational changes of the Robo1/2 ectodomain following Slit protein binding.

Our semi-quantitative RT-PCR analysis using human and mouse cDNAs indicated that the relative expression levels of the Robo2 e6b− isoform were much lower than those of the e6b+ isoform in most tissues (Figure 2). However, the expression of the e6b− isoform was relatively abundant in human spleen and mouse calvaria. To our knowledge, there is no report to date on the role of Robo2 in spleen, but we are interested in the biological role of the interaction between Robo2 and NELL1 in the calvaria.[44] During bone remodeling, the resorbing osteoclasts secrete hydrogen ions into the bone-resorbing compartment to decrease the pH to as low as 4.5.[45,46] Outside this enclosed area, the extracellular pH can drop as low as 6.0 in some pathological conditions, such as ischemia, inflammation, and the tumor microenvironment.[30] Therefore, the Robo2 e6b− isoform, which can bind to NELL1 in weakly acidic conditions (Figure 3), could enable signal transduction in a wider range of situations than the e6b+ isoform.

In summary, we have clarified the mechanism of NELL1/2-binding to Robo2 in acidic conditions. We have also identified that alternative splicing isoforms of Robo2 have different affinity for NELL1/2 in

weakly acidic conditions. Furthermore, conformational analysis of the Robo2 ectodomain using an intramolecular FRET sensor molecule and SEC analysis suggested that acidic pH does not induce an open conformation. Although the biological role of NELL1/2-Robo2 interactions remains unknown, these results provide clues to elucidate the NELL1/2-Robo2 signaling that functions in acidic conditions.

Materials and Methods

Antibodies

Mouse monoclonal antibodies against His-tag (MBL, Nagoya, Japan), HA-tag (MBL) and c-Myc-tag (Santa Cruz Biotechnology, Santa Cruz, CA) were purchased from the indicated manufacturers. Horseradish peroxidase (HRP)–conjugated anti-mouse and anti-human IgGs were purchased from Cytiva (Tokyo, Japan).

Plasmid construction

Mouse Robo2 cDNA was amplified by RT-PCR from total RNA isolated from mouse brain. This cDNA contains a microexon 6b sequences (e6b+). When investigating the constructs lacking the microexon 6b, deletions were generated by inverse PCR.

Expression vectors for mouse Robo2 ectodomain with an *N*-terminal FLAG-tag were prepared as follows: cDNAs encoding the mouse Robo2 (residues 22−863) were amplified by RT-PCR from total RNA isolated from mouse brain. The PCR products were digested with appropriate restriction enzymes, cloned into the pSecTag2-FLAG vector and designated as FLAG-Robo2-ECD. pSecTag2-FLAG was generated by subcloning annealed oligonucleotides encoding the FLAG epitope (DYKDDDDK) into the *Hind*III-*Bam*HI sites of the pSecTag2A mammalian expression vector (Invitrogen, Carlsbad, CA). Expression vectors for FNIII domains of mouse Robo2 with a *C*-terminal human immunoglobulin Fc-tag were prepared as described previously[28] and designated as Fc-Robo2-FNIII and Fc-Robo2-FNIII1. A deletion mutant lacking the coding sequence for the FNIII3 domain (residues 740–826) were generated by inverse PCR and designated as Fc-Robo2-FNIII12. An expression vector for full-length mouse Robo2 (residues 1–1512)

with a *C*-terminal HA-tag were prepared as described previously[28] and designated as Robo2-FL. An expression vector for Ig1–5 domains of mouse Robo2 with a *C*-terminal AP-tag was prepared as described previously[28] and designated as AP-Robo2-Ig. Deletion mutants lacking the coding sequence for the part of first three Ig domains (residues 43–144, 43–236, and 43–328) were generated by inverse PCR and designated as AP-Robo2-Ig2-5, AP-Robo2-Ig3-5, AP-Robo2-Ig45, respectively. The single amino acid substitution mutants (L398R) were generated by site-directed mutagenesis using inverse PCR. Expression vectors for full-length human NELL1 and NELL2 with an *N*-terminal alkaline phosphatase (AP)-tag were prepared as described previously[28] and designated as AP-NELL1 and AP-NELL2.

Expression vectors for FRET analysis were prepared as follows: mouse Robo2 ectodomain was cloned into pSecTag2A vector (Invitrogen). Acid-tolerant GFP, Gamillus (pKa = 3.4), was fused to *N*-terminus of the Robo2 ectodomain, then acid-tolerant CFP, mTurquoise2 (pKa = 3.1), was fused to *C*-terminus of Robo2-ECD to generate Gam:Robo2-ECD:mTq2 construct. cDNAs for Gamillus and mTurquoise2 were subcloned from the following plasmids. Gamillus/pcDNA3 was a gift from Takeharu Nagai (Addgene plasmid # 124837).[38] pLifeAct-mTurquoise2 was a gift from Dorus Gadella (Addgene plasmid # 36201).[37] Deletion mutants lacking the coding sequence for both the Ig1 domain (residues 43–144) and the FNIII3 domain (residues 740–826) or only Ig1 domain were generated by inverse PCR and designated as Gam:Robo2-ECD/ΔIg1&FNIII3:mTq2 and Gam:Robo2-ECD/ΔIg1:mTq2, respectively. A construct containing Cerulean/CFP fused with the Ig domains of Robo2 (22–499) was used as the negative control. A cDNA for Cerulean was subcloned from a plasmid described previously.[47] An expression vector for full-length human NELL1 with an *N*-terminal FLAG-tag was prepared as described previously.[28] The domain structures of all proteins used in this study were predicted by the simple molecular architecture research tool (SMART) program (http://smart.embl.de).[48-50]

Protein expression and purification

Recombinant NELL1/2 and Robo2 proteins were produced by the FreeStyle MAX 293 Expression System (Invitrogen), according to the manufacturer's instructions. Briefly, 293-F cells were transfected

with the expression plasmids using the FreeStyle MAX Reagent (Invitrogen) and grown in serum-free FreeStyle 293 Expression medium (Invitrogen) for 2−6 days. When necessary, recombinant proteins with hexahistidine tag were purified from the conditioned media using 1-ml HisTrap HP columns (Cytiva). Purified proteins were analyzed by sodium dodecyl sulfate–polyacrylamide gel electrophoresis (SDS-PAGE) under reducing conditions, and separated proteins were visualized by Coomassie Brilliant Blue (CBB) R-250 staining (Quick-CBB, Wako, Osaka, Japan).

Immunoblot analysis

Proteins were separated on SDS-polyacrylamide gels, followed by transfer onto Amersham Protran Premium 0.45 nitrocellulose membranes (Cytiva). The membranes were blocked with 5% (w/v) skim milk in phosphate buffered saline (PBS) containing 0.1% (v/v) Tween 20, followed by incubation with the primary antibody for 1 h at room temperature. The membranes were then washed and incubated with the HRP-conjugated secondary antibody for 1 h at room temperature. The membranes were developed with the ECL start Western Blotting Detection Reagent (Cytiva) and imaged on an LAS-4000mini Luminescent Image Analyzer (Cytiva).

Cell surface biotinylation

Cells were incubated with 1 mg/ml biotin-SS-Sulfo-OSu (Dojindo, Kumamoto, Japan) for 30 min at 4 °C for cell surface biotinylation. Cells were then washed with Tris-HCl buffer, pH 8.0, containing 0.1 mM EDTA and 150 mM NaCl, followed by solubilization with RIPA buffer (50 mM Tis-HCl, pH 7.4, 150 mM NaCl, 1% NP-40, 0.5% Sodium deoxycholate, 0.1% SDS, 1 mM EDTA). Biotinylated proteins were precipitated by streptavidin beads, resolved by SDS-PAGE, and immunoblotted with anti-HA antibody.

Cell-free binding assay

Solid-phase binding assays were performed using FLAG tag antibody plates (GenScript, Piscataway, NJ) or Protein A-coated plates (Thermo Scientific, Waltham, MA). Conditioned media or

purified proteins (approximately 80 nM) were allowed to bind to wells for 1 h at room temperature. Wells were washed three times with HBAH buffer (0.2% BSA and 20 mM HEPES, pH 7.0 in Hank's balanced salt solution), treated with conditioned media containing AP-tagged proteins for 1 h at room temperature and then washed three times with HBAH buffer. When analyzed under various pH conditions, AP-tagged proteins were diluted in 50 mM HEPES buffer (pH 7.4 and 7.0) or 50 mM MES buffer (pH range 6.8–5.5). The bound AP activity (absorbance at 405 nm/time) was measured using the Alkaline Phosphatase Yellow (pNPP) Liquid Substrate System (Sigma-Aldrich, St. Louis, MO). The apparent K_D values were calculated according to non-linear fit with one-site specific binding using GraphPad Prism 9 software (GraphPad Software, San Diego, CA).

Cell surface binding assay

Monkey kidney COS-1 cells were maintained in Dulbecco's modified Eagle's medium (DMEM) containing 10% (v/v) fetal calf serum (FCS). Transient transfection of COS-1 cells was carried out using the FuGENE HD Transfection Reagent (Promega), according to the manufacturer's instructions. Transiently transfected COS-1 cells were incubated with the conditioned media containing AP-NELL1 or AP-NELL2 (approximately 2 nM) for 90 min at room temperature. Cells were washed three times with the HBAH buffer and fixed in 4% paraformaldehyde for 15 min. Fixed cells were washed three times with 20 mM HEPES (pH 7.0)/150 mM NaCl, incubated at 65 °C for 100 min to inactivate endogenous AP, washed with AP buffer (100 mM Tris-HCl [pH 9.0], 150 mM NaCl, 1 mM $MgCl_2$) and stained with the 5-bromo-4-chloro-3-indolyl-phosphate (BCIP)-nitroblue tetrazolium (NBT) Solution Kit (Nakalai Tesque, Kyoto, Japan) at room temperature overnight.

Reverse transcription-polymerase chain reaction (RT-PCR)

RT-PCR to check for the presence of microexon 6b was performed as follows: Human total RNA samples were obtained from FirstChoice Human Total RNA Survey Panel (Invitrogen). Reverse transcription of mRNA was carried out with ReverTra Ace (Toyobo, Osaka, Japan) and random primers. Single-stranded

cDNA was amplified by PCR using GoTaq Green Master Mix (Promega, Madison, WI) under the following conditions: denaturation at 95 °C for 30 s, annealing at 60 °C for 30 s, and extension at 72 °C for 30 s; these steps were repeated for 32 (human) or 35 (mouse) cycles. The PCR products were separated by electrophoresis in 8% (w/v) acrylamide gel and stained with ethidium bromide. The oligonucleotide primers were as follows: human Robo2, 5'-GGAAGCCTCTGCTACACTCACCGTC-3' (forward) and 5'-AACAATCTGATCTCTTGGCCGAACC-3' (reverse); mouse Robo2, 5'-GGAAGCCTCTGCTACCCTCACTGTC-3' (forward) and 5'-AACGATCTGATCTCTTGGCCTAACC-3' (reverse).

***in vitro* FRET measurement**

The purified fluorescent proteins (approximately 5 μg) were diluted 5- to 10-fold (approximately 80 nM) in 50 mM HEPES buffer (pH 7.4 and 7.0) or 50 mM MES buffer (pH ranges 6.8–5.5), excited at 430 nm (λ_{max} for mTurquoise2), and emission spectra (460−560 nm) were measured by fluorospectrometer RF-5300PC (Shimadzu, Kyoto, Japan). The FRET ratio was defined as the ratio of emission intensity of Gamillus/GFP to the emission intensity of mTurquoise2/CFP (515 ± 5 nm/475 ± 5 nm).

Size exclusion chromatography (SEC)

The purified Robo2 ectodomain proteins (approximately 50~100 μg) were analyzed by size exclusion chromatography on a HiPrep 16/60 Sephacryl S-300 HR column (Cytiva) in neutral buffer (50 mM sodium phosphate buffer, pH 7.4, containing 150 mM NaCl) or acidic buffer (50 mM MES buffer, pH 5.5, containing 150 mM NaCl) using an AKTAprime plus system (Cytiva). The sample volume was 1 ml and the frow rate was 0.5 ml/min. Elution was monitored by absorbance at 280 nm. High molecular weight gel filtration calibration kits (Cytiva) were used as protein standards.

Acknowledgements: We thank Edanz Group (www.edanzediting.com/ac) for editing a draft of this manuscript. This work was supported by Japan Society for the Promotion of Science (JSPS) KAKENHI Grant Numbers 17K01946 and 20H02948.

Conflict of interest: The authors declare that they have no conflicts of interest with the contents of this article.

CRediT author contribution statement: Masaki Miyaguchi: Investigation. Yoichi Nakanishi: Methodology, Resource. Andrés D. Maturana: Validation. Kimihiko Mizutani: Validation. Tomoaki Niimi: Conceptualization, Investigation, Writing.

References

1. Rothberg, J.M., Hartley, D.A., Walther, Z., Artavanis-Tsakonas, S. (1988). slit: an EGF-homologous locus of D. melanogaster involved in the development of the embryonic central nervous system. *Cell* **55**, 1047-1059.
2. Seeger, M., Tear, G., Ferres-Marco, D., Goodman, C.S. (1993). Mutations affecting growth cone guidance in Drosophila: genes necessary for guidance toward or away from the midline. *Neuron* **10**, 409-426.
3. Ypsilanti, A.R., Zagar, Y., Chedotal, A. (2010). Moving away from the midline: new developments for Slit and Robo. *Development* **137**, 1939-1952.
4. Seiradake, E., Jones, E.Y., Klein, R. (2016). Structural perspectives on axon guidance. *Annu. Rev. Cell Dev. Biol.* **32**, 577-608.
5. Kidd, T., Brose, K., Mitchell, K.J., Fetter, R.D., Tessier-Lavigne, M., Goodman, C.S., Tear, G. (1998). Roundabout controls axon crossing of the CNS midline and defines a novel subfamily of evolutionarily conserved guidance receptors. *Cell* **92**, 205-215.
6. Li, H.S., Chen, J.H., Wu, W., Fagaly, T., Zhou, L., Yuan, W., Dupuis, S., Jiang, Z.H., Nash, W., Gick, C., Ornitz, D.M., Wu, J.Y., Rao, Y. (1999). Vertebrate slit, a secreted ligand for the transmembrane protein roundabout, is a repellent for olfactory bulb axons. *Cell* **96**, 807-818.
7. Huminiecki, L., Gorn, M., Suchting, S., Poulsom, R., Bicknell, R. (2002). Magic roundabout is a new member of the roundabout receptor family that is endothelial specific and expressed at sites of active angiogenesis. *Genomics* **79**, 547-552.
8. Liu, Z., Patel, K., Schmidt, H., Andrews, W., Pini, A., Sundaresan, V. (2004). Extracellular Ig domains 1 and 2 of Robo are important for ligand (Slit) binding. *Mol. Cell. Neurosci.* **26**, 232-240.
9. Morlot, C., Thielens, N.M., Ravelli, R.B., Hemrika, W., Romijn, R.A., Gros, P., Cusack, S., McCarthy, A.A. (2007). Structural insights into the Slit-Robo complex. *Proc. Natl. Acad. Sci. U. S. A.* **104**, 14923-14928.
10. Zelina, P., Blockus, H., Zagar, Y., Peres, A., Friocourt, F., Wu, Z., Rama, N., Fouquet, C., Hohenester, E., Tessier-Lavigne, M., Schweitzer, J., Roest Crollius, H., Chedotal, A. (2014). Signaling switch of the axon guidance receptor Robo3 during vertebrate evolution. *Neuron* **84**, 1258-1272.
11. Jaworski, A., Tom, I., Tong, R.K., Gildea, H.K., Koch, A.W., Gonzalez, L.C., Trssier-Lavigne, M. (2015). Operational redundancy in axon guidance through the multifunctional receptor Robo3 and its ligand NELL2. *Science* **350**, 961-965.

12. Pak, J.S., DeLoughery, Z.J., Wang, J., Acharya, N., Park, Y., Jaworski, A., Ozkan, E. (2020). NELL2-Robo3 complex structure reveals mechanisms of receptor activation for axon guidance. *Nat. Commun.* **11**, 1489.

13. Matsuhashi, S., Noji, S., Koyama, E., Myokai, F., Ohuchi, H., Taniguchi, S., Hori, K. (1995). New gene, nel, encoding a M(r) 93 K protein with EGF-like repeats is strongly expressed in neural tissues of early stage chick embryos. *Dev. Dyn.* **203**, 212-222.

14. Watanabe, T.K., Katagiri, T., Suzuki, M., Shimizu, F., Fujiwara, T., Kanemoto, N., Nakamura, Y., Hirai, Y., Maekawa, H., Takahashi, E. (1996). Cloning and characterization of two novel human cDNAs (NELL1 and NELL2) encoding proteins with six EGF-like repeats. *Genomics* **38**, 273-276.

15. Kuroda, S., Oyasu, M., Kawakami, M., Kanayama, N., Tanizawa, K., Saito, N., Abe, T., Matsuhashi, S., Ting, K. (1999). Biochemical characterization and expression analysis of neural thrombospondin-1-like proteins NELL1 and NELL2. *Biochem. Biophys. Res. Commun.* **265**, 79-86.

16. Ting, K., Vastardis, H., Mulliken, J.B., Soo, C., Tieu, A., Do, H., Kwong, E., Bertolami, C.N., Kawamoto, H., Kuroda, S., Longaker, M.T. (1999). Human NELL-1 expressed in unilateral coronal synostosis. *J. Bone Miner. Res.* **14**, 80-89.

17. Oyasu, M., Kuroda, S., Nakashita, M., Fujimiya, M., Kikkawa, U., Saito, N. (2000). Immunocytochemical localization of a neuron-specific thrombospondin-1-like protein, NELL2: light and electron microscopic studies in the rat brain. *Brain Res. Mol. Brain Res.* **76**, 151-160.

18. Maeda, K., Matsuhashi, S., Tabuchi, K., Watanabe, T., Katagiri, T., Oyasu, M., Saito, N., Kuroda, S. (2001). Brain specific human genes, NELL1 and NELL2, are predominantly expressed in neuroblastoma and other embryonal neuroepithelial tumors. *Neurol. Med. Chir. (Tokyo)* **41**, 582-589.

19. Zhang, X., Zara, J., Siu, R.K., Ting, K., Soo, C. (2010). The role of NELL-1, a growth factor associated with craniosynostosis, in promoting bone regeneration. *J. Dent. Res.* **89**, 865-878.

20. Li, C., Zhang, X., Zheng, Z., Nguyen, A., Ting, K., Soo, C. (2019). Nell-1 is a key functional modulator in osteochondrogenesis and beyond. *J. Dent. Res.* **98**, 1458-1468.

21. Aihara, K., Kuroda, S., Kanayama, N., Matsuyama, S., Tanizawa, K., Horie, M. (2003). A neuron-specific EGF family protein, NELL2, promotes survival of neurons through mitogen-activated protein kinases. *Brain Res. Mol. Brain Res.* **116**, 86-93.

22. Nelson, B.R., Claes, K., Todd, V., Chaverra, M., Lefcort, F. (2004). NELL2 promotes motor and sensory neuron differentiation and stimulates mitogenesis in DRG in vivo. *Dev. Biol.* **270**, 322-335.

23. Nakamoto, C., Durward, E., Horie, M., Nakamoto, M. (2019). Nell2 regulates the contralateral-versus-ipsilateral visual projection as a domain-specific positional cue. *Development* **146**, dev170704.

24. Kiyozumi, D., Noda, T., Yamaguchi, R., Tobita, T., Matsumura, T., Shimada, K., Kodani, M., Kohda, T., Fujihara, Y., Ozawa, M., Yu, Z., Miklossy, G., Bohren, K.M., Horie, M., Okabe, M., Matzuk, M.M., Ikawa, M. (2020). NELL2-mediated lumicrine signaling through OVCH2 is required for male fertility. *Science* **368**, 1132-1135.

25. Jayabal, P., Zhou, F., Lei, X., Ma, X., Blackman, B., Weintraub, S.T., Houghton, P.J., Shiio, Y. (2021). NELL2-cdc42 signaling regulates BAF complexes and Ewing sarcoma cell growth. *Cell Rep.* **36**, 109254.

26. Shen, J., James, A.W., Chung, J., Lee, K., Zhang, J.B., Ho, S., Lee, K.S., Kim, T.M., Niimi, T., Kuroda, S., Ting, K., Soo, C. (2012). NELL-1 promotes cell adhesion and differentiation via Integrinbeta1. *J. Cell. Biochem.* **113**, 3620-3628.

27. Li, C., Zheng, Z., Ha, P., Chen, X., Jiang, W., Sun, S., Chen, F., Asatrian, G., Berthiaume, E.A., Kim, J.K., Chen, E.C., Pang, S., Zhang, X., Ting, K., Soo, C. (2018). Neurexin superfamily cell membrane receptor contactin-associated protein like-4 (Cntnap4) is involved in neural EGFL-like 1 (Nell-1)-responsive osteogenesis. *J. Bone Miner. Res.* **33**, 1813-1825.

28. Yamamoto, N., Kashiwagi, M., Ishihara, M., Kojima, T., Maturana, A.D., Kuroda, S., Niimi, T. (2019). Robo2 contains a cryptic binding site for neural EGFL-like (NELL) protein 1/2. *J. Biol. Chem.* **294**, 4693-4703.

29. Barak, R., Yom-Tov, G., Guez-Haddad, J., Gasri-Plotnitsky, L., Maimon, R., Cohen-Berkman, M., McCarthy, A.A., Perlson, E., Henis-Korenblit, S., Isupov, M.N., Opatowsky, Y. (2019). Structural principles in Robo activation and auto-inhibition. *Cell* **177**, 272-285.

30. Okajima, F. (2013). Regulation of inflammation by extracellular acidification and proton-sensing GPCRs. *Cell. Signal.* **25**, 2263-2271.

31. Arnett, T.R. (2008). Extracellular pH regulates bone cell function. *J. Nutr.* **138**, 415S-418S.

32. Arnett, T.R. (2010). Acidosis, hypoxia and bone. *Arch. Biochem. Biophys.* **503**, 103-109.

33. Hazehara-Kunitomo, Y., Hara, E.S., Ono, M., Aung, K.T., Komi, K., Pham, H.T., Akiyama, K., Okada, M., Oohashi, T., Matsumoto, T., Kuboki, T. (2019). Acidic pre-conditioning enhances the stem cell phenotype of human bone marrow stem/progenitor cells. *Int. J. Mol. Sci.* **20**, 1097.

34. Johnson, V., Junge, H.J., Chen, Z. (2019). Temporal regulation of axonal repulsion by alternative splicing of a conserved microexon in mammalian Robo1 and Robo2. *Elife* **8**, e46042.

35. Piston, D.W., Kremers, G.J. (2007). Fluorescent protein FRET: the good, the bad and the ugly. *Trends Biochem. Sci.* **32**, 407-414.

36. Shinoda, H., Shannon, M., Nagai, T. (2018). Fluorescent proteins for investigating biological events in acidic environments. *Int. J. Mol. Sci.* **19**, 1548.

37. Goedhart, J., von Stetten, D., Noirclerc-Savoye, M., Lelimousin, M., Joosen, L., Hink, M.A., van Weeren, L., Gadella, T.W., Jr., Royant, A. (2012). Structure-guided evolution of cyan fluorescent proteins towards a quantum yield of 93%. *Nat. Commun.* **3**, 751.

38. Shinoda, H., Ma, Y., Nakashima, R., Sakurai, K., Matsuda, T., Nagai, T. (2018). Acid-tolerant monomeric GFP from Olindias formosa. *Cell Chem. Biol.* **25**, 330-338 e337.

39. Lohse, M.J., Bunemann, M., Hoffmann, C., Vilardaga, J.P., Nikolaev, V.O. (2007). Monitoring receptor signaling by intramolecular FRET. *Curr. Opin. Pharmacol.* **7**, 547-553.

40. Miyawaki, A. (2011). Development of probes for cellular functions using fluorescent proteins and fluorescence resonance energy transfer. *Annu. Rev. Biochem.* **80**, 357-373.

41. Zakrys, L., Ward, R.J., Pediani, J.D., Godin, A.G., Graham, G.J., Milligan, G. (2014). Roundabout 1 exists predominantly as a basal dimeric complex and this is unaffected by binding of the ligand Slit2. *Biochem. J.* **461**, 61-73.

42. Yom-Tov, G., Barak, R., Matalon, O., Barda-Saad, M., Guez-Haddad, J., Opatowsky, Y. (2017). Robo Ig4 is a dimerization domain. *J. Mol. Biol.* **429**, 3606-3616.

43. Aleksandrova, N., Gutsche, I., Kandiah, E., Avilov, S.V., Petoukhov, M.V., Seiradake, E., McCarthy, A.A. (2018). Robo1 forms a compact dimer-of-dimers assembly. *Structure* **26**, 320-328 e324.

44. Niimi, T. (2021). Roles of Slit ligands and their Roundabout (Robo) family of receptors in bone remodeling. *Adv. Exp. Med. Biol.* **21**, 143-154.

45. Silver, I.A., Murrills, R.J., Etherington, D.J. (1988). Microelectrode studies on the acid microenvironment beneath adherent macrophages and osteoclasts. *Exp. Cell Res.* **175**, 266-276.

46. Clarke, B. (2008). Normal bone anatomy and physiology. *Clin. J. Am. Soc. Nephrol.* **3 Suppl 3**, S131-139.

47. Nakanishi, Y., Iida, S., Ueoka-Nakanishi, H., Niimi, T., Tomioka, R., Maeshima, M. (2013). Exploring dynamics of molybdate in living animal cells by a genetically encoded FRET nanosensor. *PLoS One* **8**, e58175.

48. Schultz, J., Milpetz, F., Bork, P., Ponting, C.P. (1998). SMART, a simple modular architecture research tool: Identification of signaling domains. *Proc. Natl. Acad. Sci. USA* **95**, 5857-5864.

49. Letunic, I., Doerks, T., Bork, P. (2015). SMART: recent updates, new developments and status in 2015. *Nucleic Acids Res.* **43**, D257-260.

50. Letunic, I., Bork, P. (2018). 20 years of the SMART protein domain annotation resource. *Nucleic Acids Res.* **46**, D493-D496.

51. Pettersen, E.F., Goddard, T.D., Huang, C.C., Couch, G.S., Greenblatt, D.M., Meng, E.C., Ferrin, T.E. (2004). UCSF Chimera--a visualization system for exploratory research and analysis. J. Comput. Chem. 25, 1605-1612.

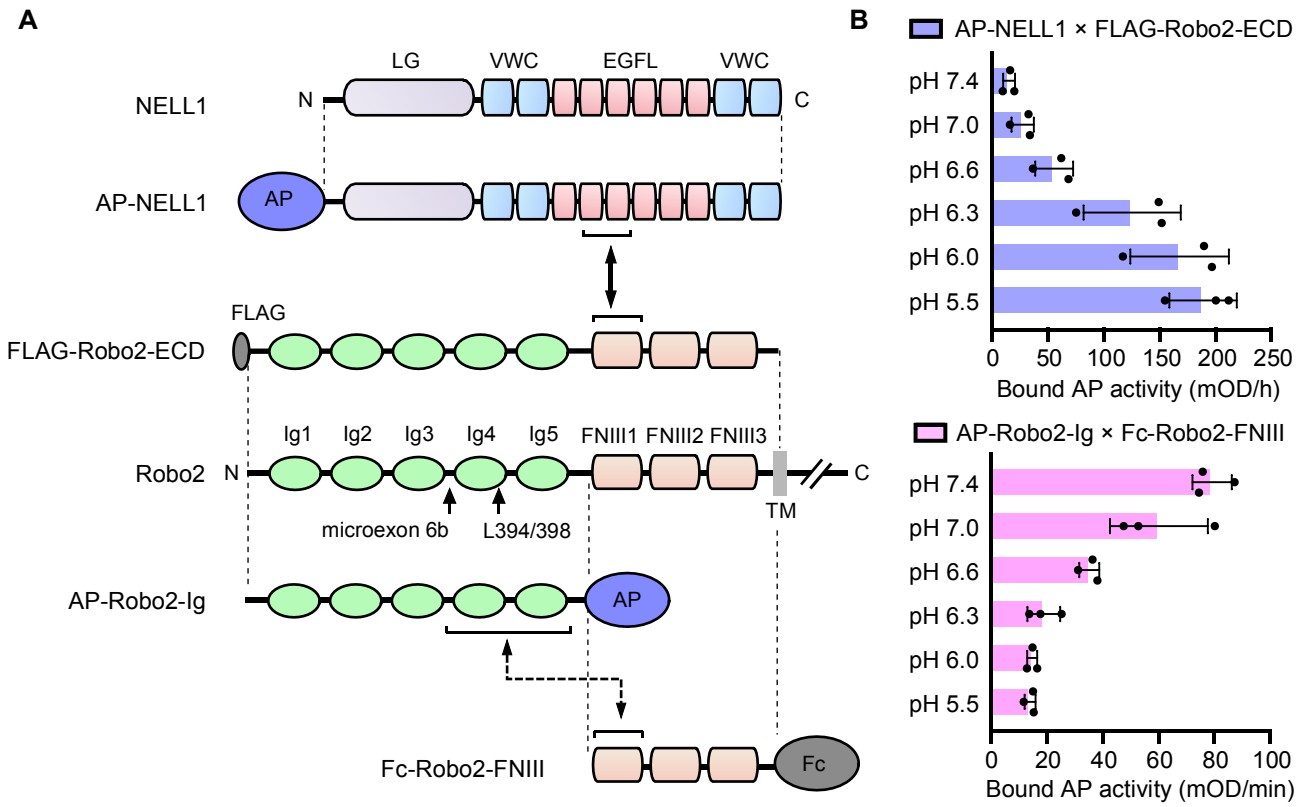

Figure 1. pH-dependent interaction of Robo2 with NELL1 and intramolecular interaction between the Ig and FNIII domains of Robo2. (A) Schematic diagrams of structural domains and epitope-tagged constructs of NELL1 and Robo2. When the cryptic NELL1-binding site is unmasked by a conformational change of the Robo2 ectodomain, the second and third EGFL domains of NELL1 bind to the FNIII1 domain of Robo2. LG, laminin G domain; VWC, von Willebrand factor type C domain; EGFL, epidermal growth factor-like domain; Ig, immunoglobulin-like domain; FNIII, fibronectin type III domain; TM, transmembrane domain. (B) Interaction between NELL1 and Robo2 (*upper* panel) or between the Robo2-Ig and Robo2-FNIII domains (*lower* panel) at the indicated pHs in solid-phase binding assays. Purified FLAG-tagged Robo2-ectodomain (ECD) was allowed to bind to anti-FLAG-coated plates and was then incubated with conditioned medium containing AP-tagged NELL1 protein. Conditioned medium containing Fc-tagged Robo2-FNIII was allowed to bind to protein A-coated plates and was then incubated with conditioned medium containing AP-tagged Robo2-Ig. The bound AP activity was measured by adding the AP substrate. Each value represents the mean ± SD of triplicate results.

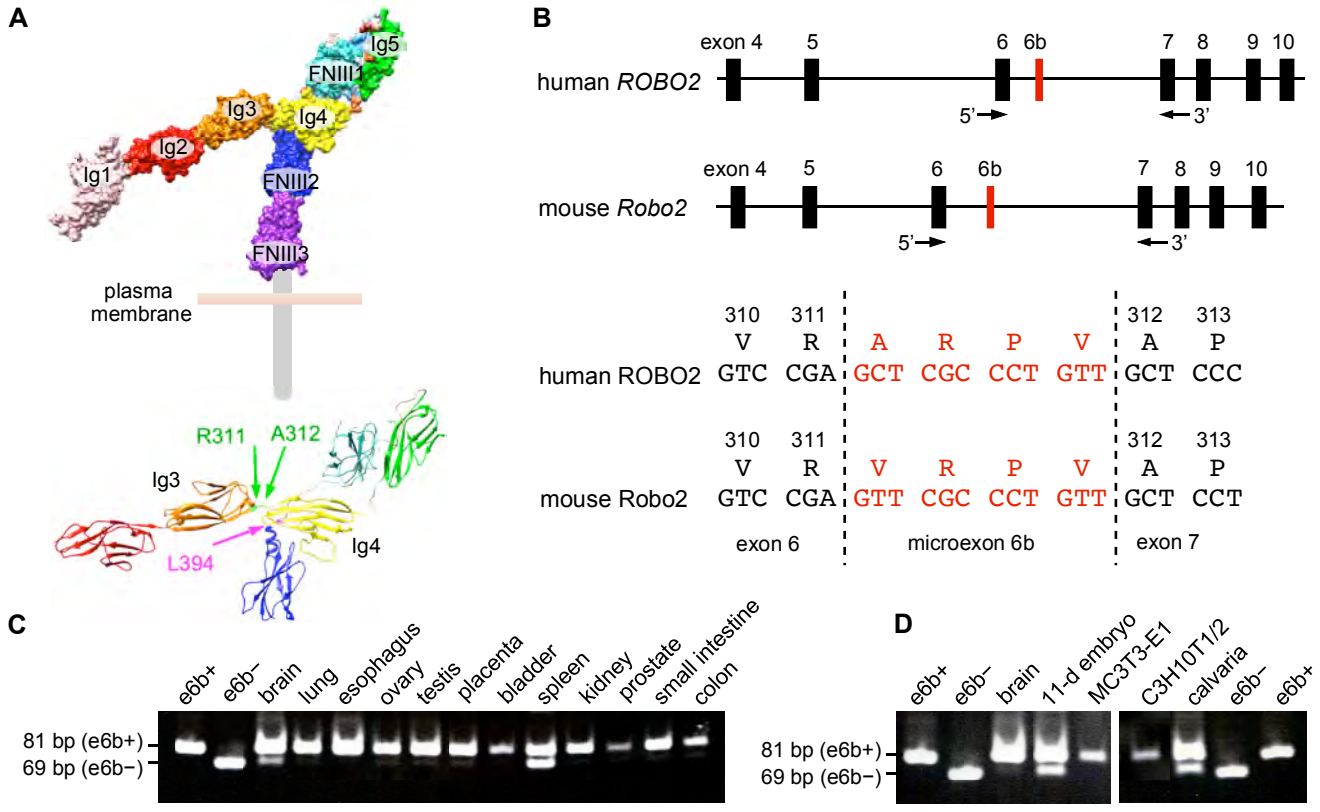

Figure 2. Alternative splicing of microexon 6b in human *ROBO2* and mouse *Robo2* genes and the expression of transcripts in various tissues. (A) The crystal structure of human ROBO2 ectodomain in surface presentation is shown on the *top* (PDB ID: 6IAA). A ribbon model of the Ig2−FNIII2 domains is shown below. Residues Arg_{311} and Ala_{312} at the boundary between exons 6 and 7 are indicated in green. Residue Leu_{394} is indicated in magenta. These images were based on the crystal structure of the e6b− isoform and generated using the program UCSF Chimera version 1.14.[45] (B) Schematic representation of the genomic structures around microexon 6b in the human *ROBO2* and mouse *Robo2* genes. Positions of oligonucleotide primers used in semi-quantitative RT-PCR are indicated by arrows. An alignment of cDNA and amino acid sequences of the exon 6/microexon 6b/exon 7 junction is shown below. Microexon 6b (12 bp) encodes a linker sequence between the Ig3 and Ig4 domains. (C and D) Semi-quantitative RT-PCR to assess the levels of e6b+ and e6b− transcripts in total RNAs from human (C) and mouse (D) tissues and cell lines. Alternative splicing of microexon 6b produces an 81-bp (e6b+) or 69-bp (e6b−) fragment.

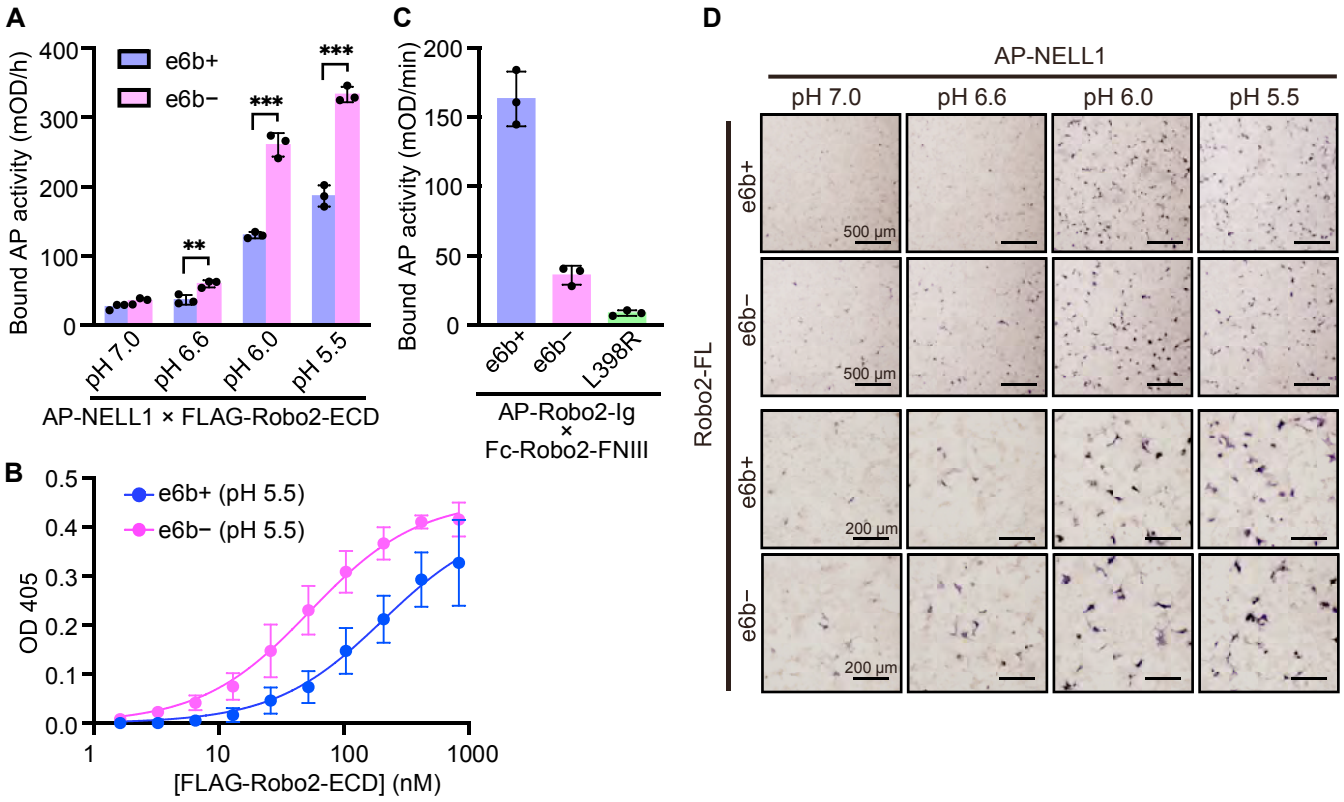

Figure 3. The Robo2 e6b− splicing isoform shows higher affinity for NELL1 than the e6b+ isoform in acidic conditions. (A) Interaction between NELL1 and Robo2 at the indicated pHs in solid-phase binding assays. Purified FLAG-Robo2-ECD isoform proteins (e6b+ or e6b−) were allowed to bind to anti-FLAG-coated plates and were then incubated with conditioned medium containing AP-tagged NELL1. The bound AP activity was measured by adding the AP substrate. Each value represents the mean ± SD of triplicate results. **, $p < 0.01$; ***, $p < 0.001$ (Student's *t*-test). (B) Titration curves of Robo2-ECD bound to NELL1 at pH 5.5. Purified FLAG-Robo2-ECD isoform proteins (e6b+ or e6b−) were allowed to bind to anti-FLAG-coated plates at various concentrations and were then incubated with conditioned medium containing AP-tagged NELL1. The bound AP activity was measured as above. (C) Interaction between the Robo2-Ig and Robo2-FNIII domains in the solid-phase binding assay. Conditioned medium containing Fc-tagged Robo2-FNIII was allowed to bind to protein A-coated plates and was then incubated with conditioned medium containing AP-tagged Robo2-Ig isoforms (e6b+ or e6b−) or the e6b+ L398R mutant (e6b+). The bound AP activity was measured as above. (D) COS-1 cells were transiently transfected with expression plasmids for Robo2-FL isoforms (e6b+ or e6b−) and incubated with conditioned medium containing AP-tagged NELL1 at the indicated pHs. The bound AP was visualized by *in situ* staining with BCIP/NBT. Scale bars, 500 μm (*upper* panels); 200 μm (*lower* panels).

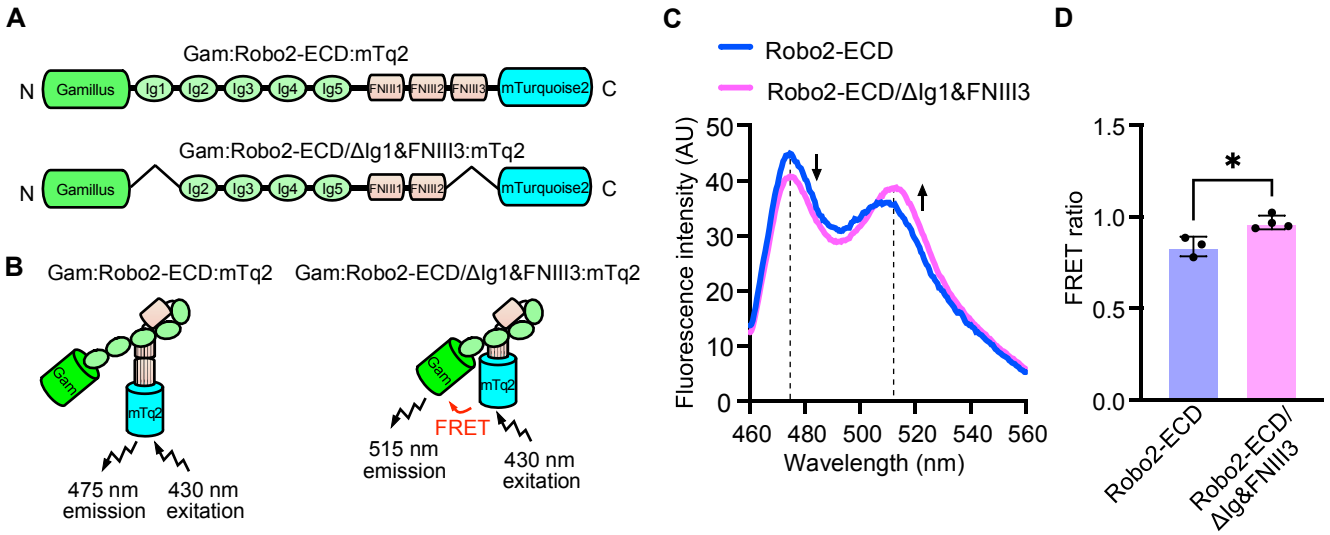

Figure 4. FRET-based indicators to assess the topological conformation of the Robo2 ectodomain. (A) Schematic diagrams of the intramolecular FRET constructs. Gamillus/GFP and mTurquoise2/CFP were fused to the *N*- and *C*-termini of the Robo2 ectodomain, respectively. A deletion construct of both the Ig1 and FNIII3 domains was prepared to decrease the distance between Gamillus and mTurquoise2. (B) Schematic overview of the FRET experiments. If Gamillus and mTurquoise2 are in close proximity due to conformational change of the Robo2 ectodomain, FRET (emission of 515-nm light after excitation with 430-nm light) may occur. (C) Emission scans of Robo2-ECD and Robo2-ECD/ΔIg1&FNIII3 constructs. The excitation wavelength was 430 nm and emission was measured at 460−560 nm. (D) The FRET ratio was defined as the ratio of emission intensity of Gamillus to the emission intensity of mTurquoise2 (515 ± 5 nm/475 ± 5 nm). Each value represents the mean ± SD of at least triplicate results. *, $p < 0.05$ (Student's *t*-test).

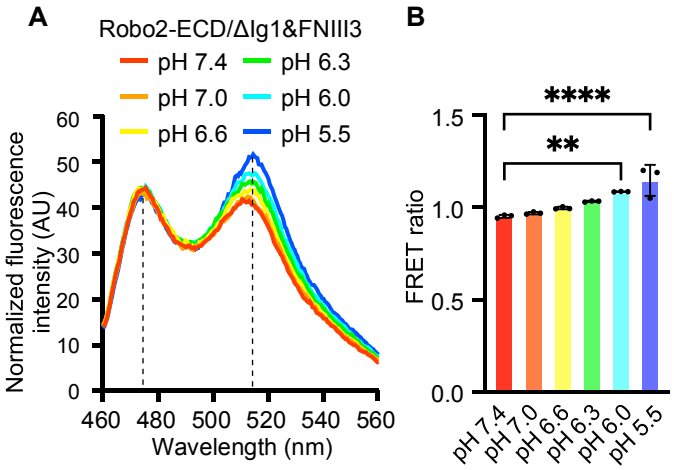

Figure 5. pH-dependent changes in FRET ratio of the Robo2-ECD/ΔIg1&FNIII3 construct. (A) Emission scans of the Robo2-ECD/ΔIg1&FNIII3 construct at the indicated pHs. All the emission spectra for CFP were normalized to have equal intensity. (B) pH-dependent changes in FRET ratio. Each value represents the mean ± SD of triplicate results. Significant differences (****, $p < 0.0001$; **, $p < 0.01$) between neutral (pH 7.4) and acidic (pH 6.0 and 5.5) conditions were determined by one-way analysis of variance (ANOVA) followed by Dunnett's *post-hoc* test.

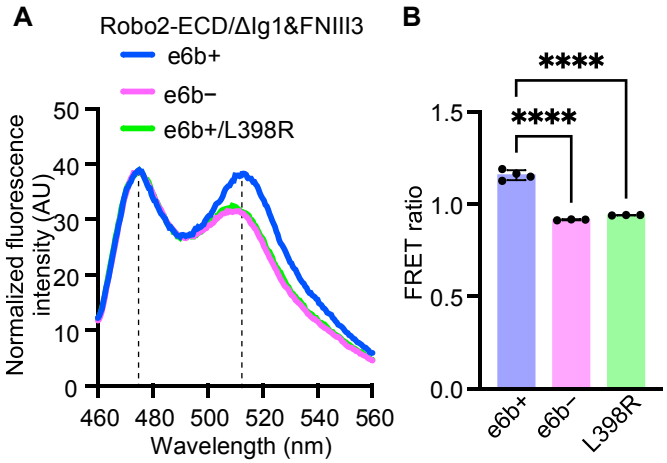

Figure 6. Decreases in FRET ratio of the Robo2-ECD/ΔIg1&FNIII3 construct for the e6b− splicing isoform. (A) Emission scans of the Robo2-ECD/ΔIg1&FNIII3 constructs for splicing isoforms (e6b+ or e6b−) and the e6b+ L398R mutant. All the emission spectra for CFP were normalized to have equal intensity. (B) Decrease in FRET ratios for the e6b− isoform and the e6b+ L398R mutant compared with that for the wild-type e6b+ isoform. Each value represents the mean ± SD of at least triplicate results. Significant differences (****, $p < 0.0001$) between the e6b+ isoform and the e6b− isoform or the e6b+ L398R mutant were determined by one-way ANOVA followed by Dunnett's *post-hoc* test.

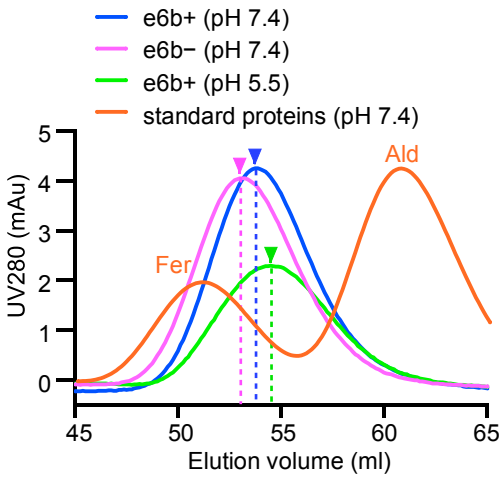

Figure 7. Size exclusion chromatography (SEC) of Robo2-ECD proteins (e6b+ or e6b−) in neutral or acidic conditions. SEC profiles of: Robo2-ECD (e6b+, pH 7.4); Robo2-ECD (e6b−, pH 7.4); Robo2-ECD (e6b+, pH 5.5); and standard proteins. Fer, ferritin (440 kDa); Ald, aldolase (158 kDa).

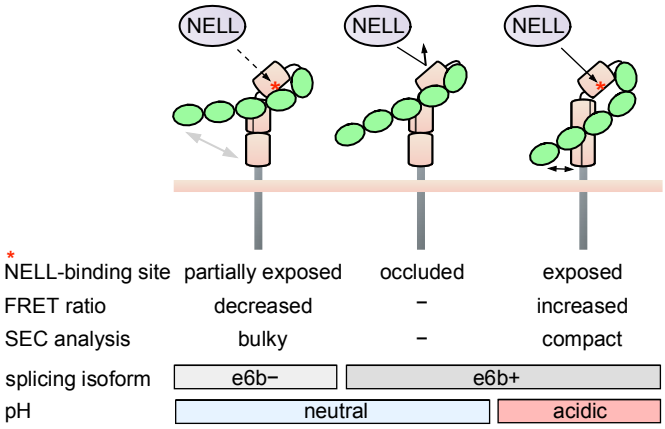

Figure 8. Summary of this study and putative conformation of the Robo2 ectodomain. At neutral pH, the Robo2 ectodomain (e6b+) forms a closed hairpin-like conformation in which the Ig4 and Ig5 domains mask the FNIII1 domain. In acidic conditions, the Robo2 ectodomain (e6b+) forms a loosened hairpin-like compact conformation in which the NELL1/2-binding site is exposed. The Robo2 e6b− isoform has a more twisted hairpin-like conformation, in which the NELL1/2-binding site is partially exposed at neutral pH.

Supplemental information

Conformational Change of the Hairpin-like-structured Robo2 Ectodomain Allows NELL1/2 Binding

Masaki Miyaguchi[1], Yoichi Nakanishi[1], Andrés D. Maturana[1], Kimihiko Mizutani[2], and Tomoaki Niimi[1]*

[1]Graduate School of Bioagricultural Sciences, Nagoya University, Nagoya, Japan

[2]Graduate School of Agriculture, Kyoto University, Kyoto, Japan

*Correspondence to be addressed to : Tomoaki Niimi, Graduate School of Bioagricultural Sciences, Nagoya University, Furo-cho, Chikusa-ku, Nagoya 464-8601, Japan; tniimi@agr.nagoya-u.ac.jp; Tel. 81-52-789-5015

Abbreviations: ECD, ectodomain; EGFL, epidermal growth factor-like; FNIII, fibronectin type III; FRET, Förster resonance energy transfer; Ig, immunoglobulin-like; LG, laminin G; NELL, neural epidermal growth factor-like (NEL)-like; Robo, Roundabout; SEC, size exclusion chromatography; VWC, von Willebrand factor type C

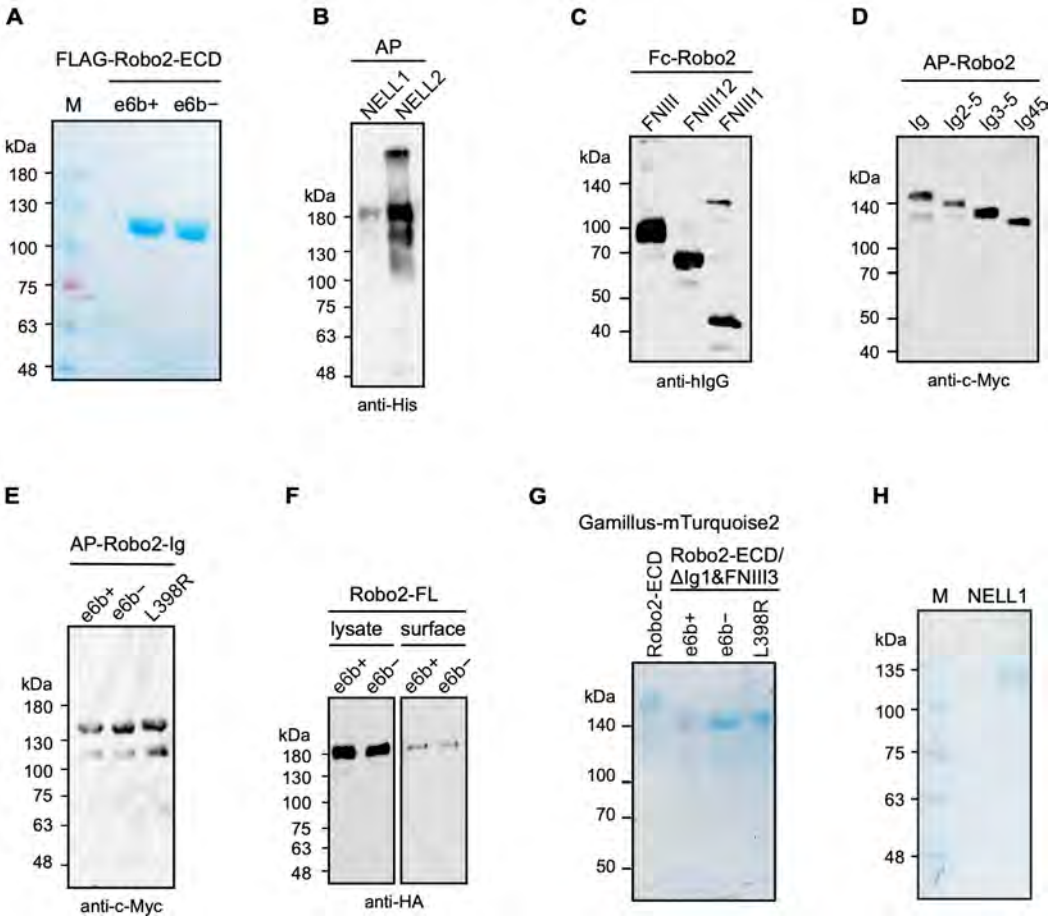

Figure S1. Preparation of fusion proteins used in this study. (A) Purified FLAG-Robo2-ECD proteins (e6b+ and e6b−) were resolved by SDS-PAGE following CBB staining. (B) AP-NELL1 and AP-NELL2 were expressed in 293-F cells. Conditioned media were resolved by SDS-PAGE and visualized by immunoblotting with the anti-His antibody. (C) Fc-Robo2-FNIII and its deletion mutants (-FNIII12 and -FNIII1) were expressed in 293-F cells. Conditioned media were resolved by SDS-PAGE and visualized by immunoblotting with the anti-human IgG antibody. (D) AP-Robo2-Ig and its deletion mutants (-Ig2-5, -Ig3-5, and -Ig45) were expressed in 293-F cells. Conditioned media were resolved by SDS-PAGE and visualized by immunoblotting with the anti-c-Myc antibody. (E) AP-Robo2-Ig proteins (e6b+ and e6b−) and its L398R mutant (e6b+) were expressed in 293-F cells. Conditioned media were resolved by SDS-PAGE and visualized by immunoblotting with the anti-c-Myc antibody. (F) Expression vectors for *C*-terminally HA-tagged Robo2-FL proteins (e6b+ and e6b−) were transfected into 293-F cells. Total cell lysates and cell surface proteins were resolved by SDS-PAGE and visualized by immunoblotting with the anti-HA antibody. (G) Purified Robo2-ECD (e6b+) and Robo2-ECD/ΔIg1&FNIII3 (e6b+, e6b−, and L398R) proteins for FRET experiment were resolved by SDS-PAGE following CBB staining. (H) Purified full-length NELL1 protein for FRET experiment was resolved by SDS-PAGE following CBB staining.

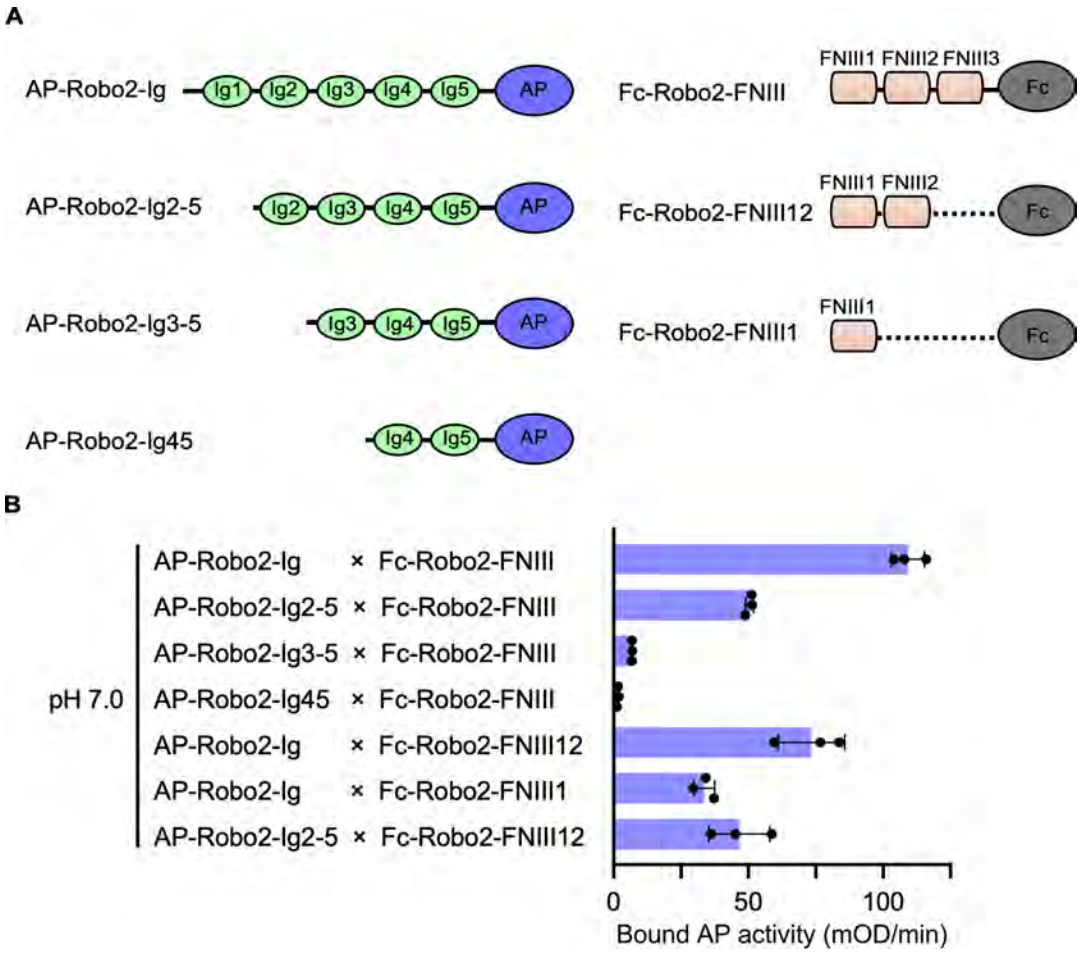

Figure S2. Identification of the binding domains for the interaction between the Ig and the FNIII domains of Robo2. (A) Schematic diagrams of the AP-tagged Robo2-Ig and the Fc-tagged Robo2-FNIII fragments. (B) Interaction between the Robo2-Ig and Robo2-FNIII domains at pH 7.0 in solid-phase binding assays. Conditioned medium containing Fc-tagged Robo2-FNIII fragments was allowed to bind to protein A-coated plates and was then incubated with conditioned medium containing AP-tagged Robo2-Ig fragments. The bound AP activity was measured by adding the AP substrate. Each value represents the mean ± SD of triplicate results.

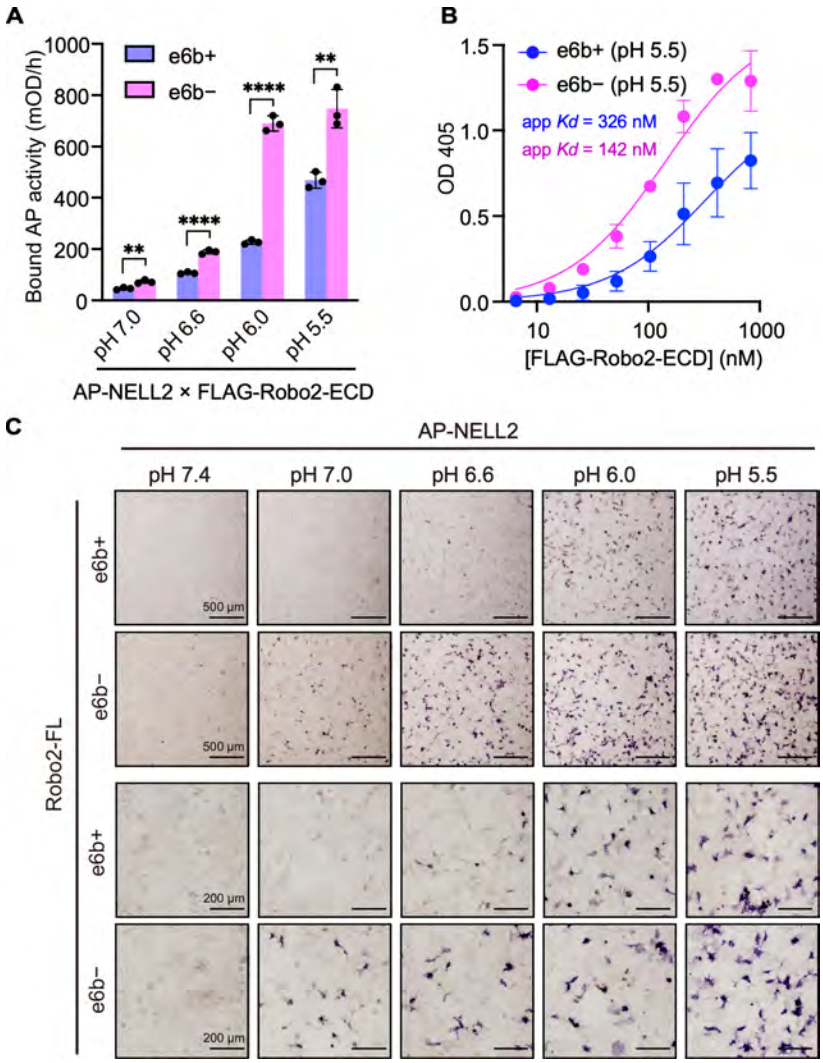

Figure S3. The Robo2 e6b− splicing isoform shows higher affinity for NELL2 than the e6b+ isoform in acidic conditions. (A) Interaction between NELL2 and Robo2 at the indicated pHs in solid-phase binding assays. Purified FLAG-Robo2-ECD isoform proteins (e6b+ or e6b−) were allowed to bind to anti-FLAG-coated plates and were then incubated with conditioned medium containing AP-tagged NELL2. The bound AP activity was measured by adding the AP substrate. Each value represents the mean ± SD of triplicate results. **, $p < 0.01$; ****, $p < 0.0001$ (Student's *t*-test). (B) Titration curves of Robo2-ECD bound to NELL2 at pH 5.5. Purified FLAG-Robo2-ECD isoform proteins (e6b+ or e6b−) were allowed to bind to anti-FLAG-coated plates at various concentrations and were then incubated with conditioned medium containing AP-tagged NELL2. The bound AP activity was measured as above. (C) COS-1 cells were transiently transfected with expression plasmids for Robo2-FL isoforms (e6b+ or e6b−) and incubated with conditioned medium containing AP-tagged NELL2 at the indicated pHs. The bound AP was visualized by *in situ* staining with BCIP/NBT. Scale bars, 500 μm (*upper* panels); 200 μm (*lower* panels).

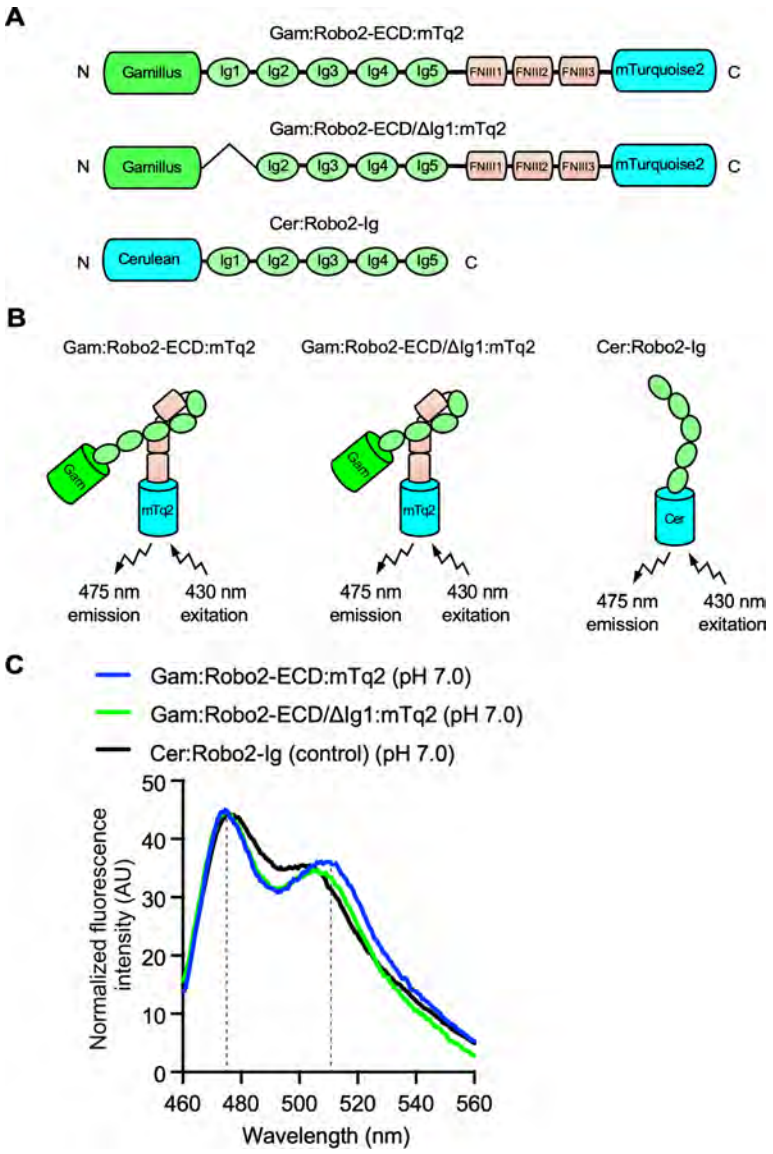

Figure S4. FRET-based indicators to assess the topological conformation of the Robo2 ectodomain. (A) Schematic diagrams of the intramolecular FRET constructs. Gamillus/GFP and mTurquoise2/CFP were fused to the *N*- and *C*-termini of the Robo2 ectodomain, respectively. A deletion construct of the Ig1 domain was prepared to decrease the distance between Gamillus and mTurquoise2. A construct containing Cerulean/CFP fused with the Ig domains of Robo2 was used as a negative control. (B) Schematic overview of the FRET experiments. FRET was not observed probably because of a poor spatial arrangement of two fluorophores. (C) Emission scans of Robo2-ECD, Robo2-ECD/ΔIg1, and control constructs at pH 7.0. The excitation wavelength was 430 nm and emission was measured at 460−560 nm. All the emission spectra for CFP were normalized to have equal intensity.

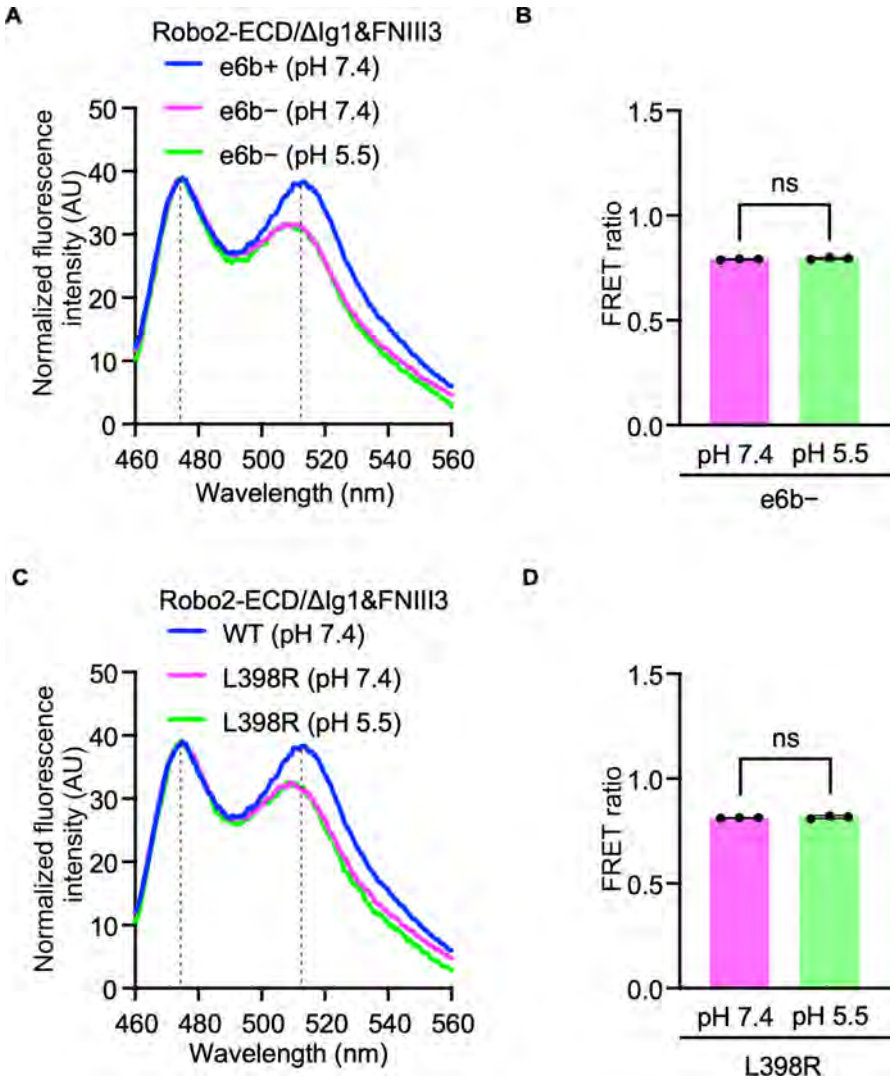

Figure S5. Acidic pH did not change in FRET ratio of the Robo2-ECD/ΔIg1&FNIII3 construct for the e6b− splicing isoform and the e6b+ L398R mutant. (A) Emission scans of the Robo2-ECD/ΔIg1&FNIII3 constructs for the e6b+ isoform (pH 7.4) and the e6b− isoform (pH 7.4 and 5.5). All the emission spectra for CFP were normalized to have equal intensity. (B) No significant change in FRET ratio for the Robo2-ECD/ΔIg1&FNIII3 construct for the e6b− isoform at the indicated pHs. Each value represents the mean ± SD of at least triplicate results. ns, not significant (Student's *t*-test). (C) Emission scans of the Robo2-ECD/ΔIg1&FNIII3 construct for the e6b+ wild-type (pH 7.4) and the e6b+ L398R mutant (pH 7.4 and 5.5). All the emission spectra for CFP were normalized to have equal intensity. (D) No significant change in FRET ratio of the Robo2-ECD/ΔIg1&FNIII3 construct for the e6b+ L398R mutant at the indicated pHs. Each value represents the mean ± SD of at least triplicate results. ns, not significant (Student's *t*-test).

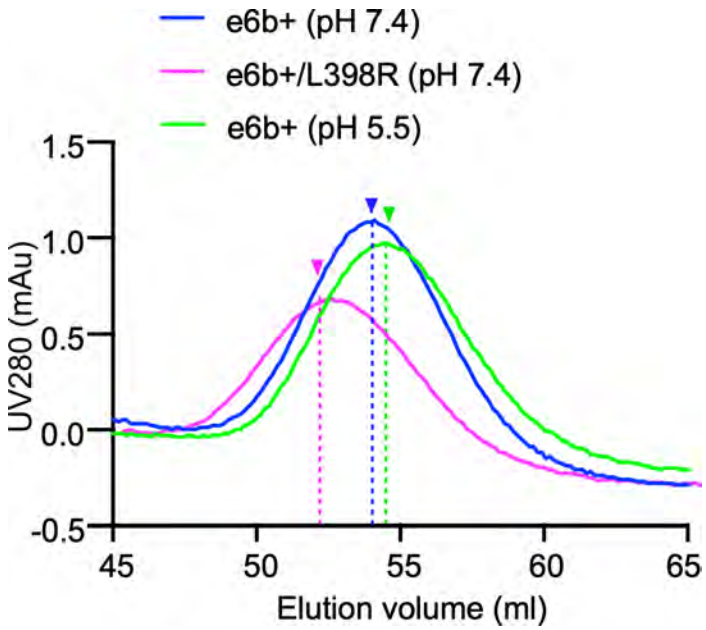

Figure S6. Size exclusion chromatography of Robo2-ECD protein (e6b+) and its L398R mutant in neutral or acidic conditions. SEC profiles of: Robo2-ECD (e6b+, pH 7.4); Robo2-ECD (e6b+ L398R, pH 7.4); and Robo2-ECD (e6b+, pH 5.5).

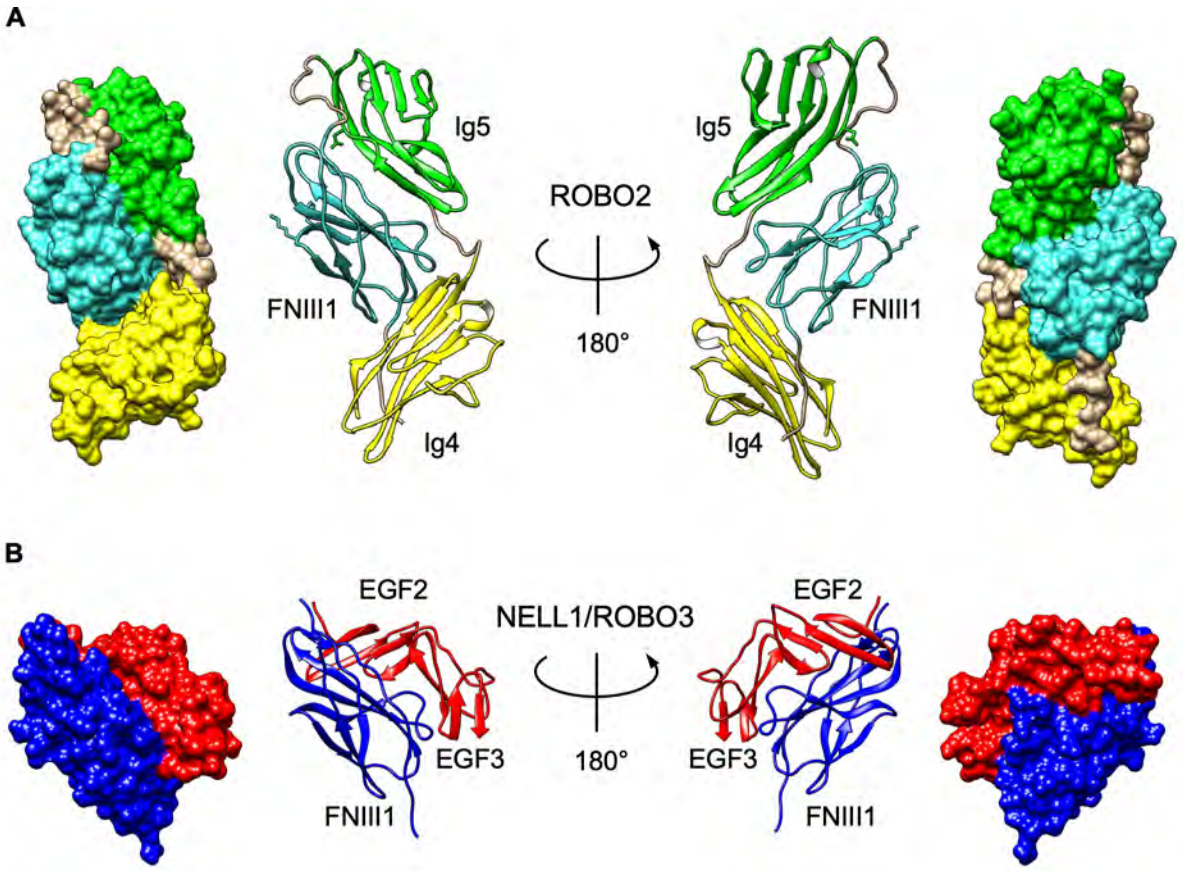

Figure S7. Comparison of the structure around the folded ROBO2-FNIII1 domain and the NELL1-binding site of the ROBO3-FNIII1 domain. (A) The crystal structure of human ROBO2 ectodomain around FNIII1 domain (PDB ID: 6IAA). (B) The crystal structure of human ROBO3 FNIII1 domain (blue) bound to human NELL1 EGF2-3 domains (red) (PDB ID: 6POL). These images were generated using the program UCSF Chimera version 1.14.[51]

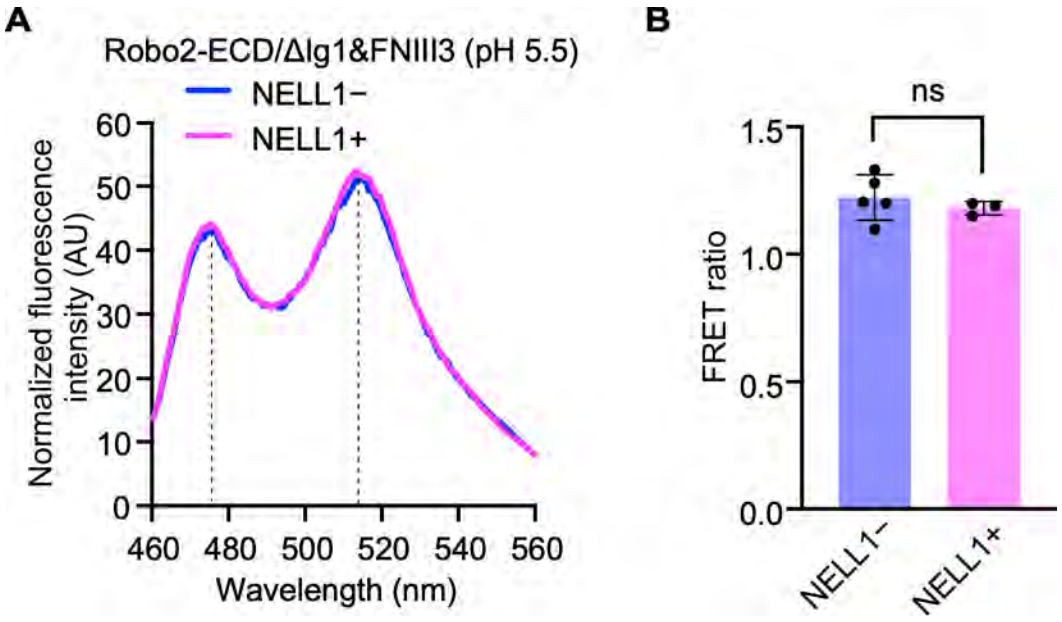

Figure S8. No significant change in FRET ratio of the Robo2-ECD/ΔIg1&FNIII3 construct in the presence or absence of NELL1 protein. (A) Emission scans of the Robo2-ECD/ΔIg1&FNIII3 construct at pH 5.5 in the presence or absence of NELL1 protein (approximately 80 nM; up to 25% of Robo2 can bind to NELL1). All the emission spectra for CFP were normalized to have equal intensity. (B) No significant change in FRET ratio. Each value represents the mean ± SD of at least triplicate results. ns, not significant (Student's *t*-test).